Contribution from the Department of Chemistry, University of Florence, Florence, Italy, and Laboratoire de Chimie (UA CNRS 1194), Department de Recherche Fondamentale, Centre d'Etudes Nucleaires, Grenoble, France

Structure and Magnetic Properties of Two Bis(nitronyl nitroxide) Adducts of Bis(hexafluoroacetylacetonato)manganese(II). Molecular Orbital Interpretation of the Coupling in Manganese–Nitroxide Complexes

A. Caneschi,† D. Gatteschi,*† J. Laugier,‡ L. Pardi,† P. Rey,*‡ and C. Zanchini†

Received October 20, 1987

Two new bis adducts were obtained by reaction of manganese hexafluoroacetylacetonate, $Mn(hfac)_2$, with the nitronyl nitroxide ligands 2,4,4,5,5-pentamethyl-4,5-dihydro-1*H*-imidazolyl-1-oxy 3-oxide, NITMe, and 2-phenyl-4,4,5,5-tetramethyl-4,5-dihydro-1*H*-imidazolyl-1-oxy 3-oxide, NITPh. The X-ray crystal structure showed that $Mn(hfac)_2(NITPh)_2$ (II) is monoclinic, space group $P2_1/c$, with a = 12.343 (6) Å, b = 15.474 (7) Å, c = 22.47 (1) Å, β = 100.03 (2)°, and Z = 4, and $Mn(hfac)_2(NITMe)_2$ (I) is monoclinic, space group $P2_1/n$, with a = 17.235 (8) Å, b = 17.679 (7) Å, c = 11.446 (5) Å, β = 90.73 (2)°, nd Z = 4. The magnetic properties of both complexes have been studied by static susceptibility and EPR techniques. The manganese(II) ions and the radicals are antiferromagnetically coupled, with a ground quartet state. An extended Hückel formalism has been used to establish structural–magnetic correlations in manganese–nitroxide complexes.

Introduction

In the course of systematic attempts to synthesize low-dimensional magnetic materials by using paramagnetic ligands,[1-5] like the nitroxides, we focused our attention on nitronyl nitroxides, NITR, which, having two equivalent coordination sites, can easily form chains.[4,5] A particular interest was devoted to manganese(II) complexes, which can yield ferrimagnetic chains.

Beyond several chain compounds, we obtained also some mononuclear metal derivatives of formula $Mn(hfac)_2(NITR)_2$, (hfac = hexafluoroacetylacetonate) where R can be either phenyl, giving the ligand 2-phenyl-4,4,5,5-tetramethyl-4,5-dihydro-1*H*-imidazolyl-1-oxy 3-oxide (NITPh), or methyl, giving the ligand 2,4,4,5,5-pentamethyl-4,5-dihydro-1*H*-imidazolyl-1-oxy 3-oxide (NITMe). The structure and magnetic properties of two adducts with the same stoichiometry have been previously reported[6,7] with the nitroxides 2,2,6,6-tetramethylpiperidinyl-1-oxy (TEMPO), and 2,2,5,5-tetramethylpyrrolidinyl-1-oxy (PROXYL), in which the manganese(II) ion is antiferromagnetically coupled to the two radicals with coupling constants J = 158 cm^{-1} for the former and J = 210 cm^{-1} for the latter. In both cases the complexes can be described as trans adducts of manganese(II) hexafluoroacetylacetonate.

We have found that $Mn(hfac)_2(NITPh)_2$ has a structure very similar to those of the TEMPO and PROXYL derivatives, while $Mn(hfac)_2(NITMe)_2$ is a cis rather than a trans adduct. We wish to report here the structure and the magnetic properties of the NITR derivatives and to compare the values of the manganese–radical coupling constants in the four complexes thus far characterized by using extended Hückel calculations similar to those previously reported, which allowed us to establish structural magnetic correlations in copper(II) complexes.[8]

Experimental Section

Synthesis of the Complexes. The NITPh and NITMe radicals,[9,10] as well as $Mn(hfac)_2 \cdot 2H_2O$,[11] were prepared according to established procedure. $Mn(hfac)_2(NITPh)_2$ and $Mn(hfac)_2(NITMe)_2$ were synthesized by following the same procedure: 1 mmol of the manganese(II) salt was dissolved in 60 mL of dry boiling *n*-heptane; after 10 min, the solution was allowed to cool down to 80 °C and mixed, under stirring, with a solution of 2.2 mmol of the radical dissolved in 20 mL of dry *n*-heptane at 60 °C. The final solution was filtered, allowed to cool down to 20 °C and filtered again after 6 h to separate from an oil, and, finally, stored at −10 °C. Nice dark green crystals for the NITPh derivative and red wine crystals for the NITMe one were obtained after 24 h. The compounds analyzed satisfactorily for $Mn(hfac)_2(NITPh)_2$ (Anal. Calcd for $MnC_{36}H_{36}O_8F_{12}N_4$: C, 46.15; H, 3.85; N, 5.98; Mn, 5.88. Found: C, 46.32; H, 3.98; N, 6.11; Mn, 5.61) and $Mn(hfac)_2(NITMe)_2$ (Anal. Calcd for $MnC_{26}H_{32}O_8F_{12}N_4$: C, 38.47; H, 3.99; N, 6.90. Found: C, 38.32; H, 3.96; N, 6.77), respectively.

X-ray Data Collection and Reduction. X-ray data for $Mn(hfac)_2(NITMe)_2$ and $Mn(hfac)_2(NITPh)_2$ were collected on an Enraf-Nonius CAD-4 four-circle diffractometer with Mo Kα radiation. Accurate unit cell parameters were derived from least-squares refinement of the setting

Table I. Crystallographic Data and Experimental Parameters for $Mn(hfac)_2(NITMe)_2$ (I) and $Mn(hfac)_2(NITPh)_2$ (II)

	I	II
formula	$C_{26}H_{32}MnO_8N_4F_{12}$	$C_{36}H_{36}MnO_8N_4F_{12}$
mol wt	811.48	935.62
cryst syst	monoclinic	monoclinic
space group	$P2_1/n$	$P2_1/c$
cell params		
a, Å	17.235 (8)	12.343 (6)
b, Å	17.679 (7)	15.474 (7)
c, Å	11.446 (5)	22.47 (1)
β, deg	90.73 (2)	100.03 (2)
V, Å^3	3487.1	4225.9
Z	4	4
d(calcd), g cm^{-3}	1.55	1.47
linear abs (V), mm^{-1}	0.5	0.4
cryst size, mm	0.30 × 0.20 × 0.20	0.25 × 0.25 × 0.20
temp., °C	20	20
radiation		
takeoff angle, deg	6	6
λ, Å	0.7107 (Mo Kα)	0.7107 (Mo Kα)
monochromator	graphite	graphite
bragg angle, deg	$1 < \theta < 25$	$1 < \theta < 25$
scan mode	ω	ω
scan range, deg	0.6 + 0.35 tan θ	0.6 + 0.35 tan θ
scan speed, deg/min	0.6–4	0.6–4
detector window		
height, mm	4	4
width, mm	2.40 + 3.3 tan θ	3.0 + 3.5 tan θ
test refcns	(−3.3,4), (073)	(436), (−1,0,12)
measd reflcns	$-20 < h < 20$, $0 < k < 21$, $0 < l < 13$	$-14 < h < 14$, $0 < k < 18$, $0 < l < 26$
tot. no. of reflcns	6750	7438
no. of reflcns with $F > 4\sigma(F)$	2537	2868

(1) Benelli, C.; Caneschi, A.; Gatteschi, D.; Rey, P. In *Organic and Inorganic Low Dimensional Crystalline Materials*; Delhaes, P., Drillon, M., Eds.; NATO ASI Series; Plenum: New York, 1987.
(2) Caneschi, A.; Gatteschi, D.; Laugier, J.; Rey, P. In *Organic and Inorganic Low Dimensional Crystalline Materials*; Delhaes, P., Drillon, M., Eds.; NATO ASI Series; Plenum: New York, 1987.
(3) Caneschi, A.; Gatteschi, D.; Laugier, J.; Rey, P.; Sessoli, R.; Zanchini, C. In *Organic and Inorganic Low Dimensional Crystalline Materials*; Delhaes, P., Drillon, M., Eds.; NATO ASI Series; Plenum: New York, 1987.
(4) Caneschi, A.; Gatteschi, D.; Laugier, J.; Rey, P. *J. Am. Chem. Soc.* **1987**, *109*, 2191.
(5) Laugier, J.; Rey, P.; Benelli, C.; Gatteschi, D.; Zanchini, C. *J. Am. Chem. Soc.* **1986**, *108*, 6931.
(6) Dickman, M. H.; Porter, L. C.; Doedens, R. J. *Inorg. Chem.* **1986**, *25*, 2595.
(7) Benelli, C.; Gatteschi, D.; Zanchini, C.; Doedens, R. J.; Dickman, M. H.; Porter, L. C. *Inorg. Chem.* **1986**, *25*, 3453.
(8) Caneschi, A.; Gatteschi, D.; Grand, A.; Laugier, J.; Pardi, L.; Rey, P., submitted for publication.

† University of Florence.
‡ Centre d'Etudes Nucleaires.

0020-1669/88/1327-2027$01.50/0

Table II. Positional Parameters ($\times 10^4$) and Temperature Factors ($Å^2 \times 10^3$) for the NITMe Adduct[a]

	x	y	z	B_{eq}
MN	2292 (1)	220 (1)	1884 (1)	3.95
O1	2450 (3)	728 (3)	192 (4)	4.95
O2	2308 (3)	−801 (3)	839 (5)	5.30
C1	2493 (5)	432 (5)	−785 (7)	4.79
C2	2679 (8)	989 (7)	−1758 (9)	7.30
C3	2433 (5)	−315 (5)	−1076 (7)	5.57
C4	2323 (5)	−873 (5)	−244 (8	4.75
C5	2221 (11)	−1662 (7)	−683 (11)	8.69
F1	2185 (6)	1542 (5)	−1783 (7)	13.26
F2	3338 (5)	1256 (6)	−1689 (7)	17.86
F3	2587 (5)	713 (5)	−2803 (5)	12.88
F4	2143 (7)	−1768 (4)	−1755 (7)	16.16
F5	2822 (7)	−2056 (5)	−438 (11)	19.97
F6	1700 (8)	−2016 (6)	−235 (12)	22.58
O3	2122 (3)	−379 (3)	3521 (4)	4.91
O4	1047 (3)	121 (3)	1817 (5)	5.42
C6	1520 (6)	−682 (4)	3906 (7)	4.53
C7	1639 (9)	−1083 (6)	5068 (8)	7.29
C8	796 (6)	−695 (5)	3422 (8)	5.61
C9	617 (5)	−290 (5)	2398 (8)	5.09
C10	−189 (7)	−360 (7)	1900 (11)	7.49
F7	2272 (6)	−953 (7)	5551 (7)	18.69
F8	1569 (5)	−1786 (4)	5014 (6)	12.14
F9	1137 (7)	−886 (5)	5823 (6)	16.49
F10	5221 (5)	4222 (5)	4004 (7)	13.03
F11	−478 (4)	269 (5)	1544 (9)	14.09
F12	−694 (4)	−645 (6)	2593 (7)	16.06
O5	2262 (3)	1317 (3)	2635 (4e	4.39
O6	368 (4)	2353 (4)	4919 (5)	7.10
N1	1647 (4)	1717 (3)	2928 (5)	3.81
N2	775 (4)	2217 (4)	4013 (6)	5.05
C11	1349 (5)	1704 (4)	3975 (6)	4.19
C12	1600 (5)	1238 (5)	4968 (7)	5.80
C13	612 (5)	2577 (4)	2859 (7)	4.70
C14	−150 (6)	2256 (6)	2423 (9)	8.51
C15	551 (6)	3437 (5)	3013 (9)	7.58
C16	1324 (5)	2322 (4)	2151 (6)	4.40
C17	1957 (6)	2926 (5)	2058 (10	8.40
C18	1140 (7)	1994 (6)	955 (7)	8.43
O7	3506 (3)	142 (3)	2219 (4)	4.43
O8	4978 (4)	1367 (4)	5010 (5)	7.85
N3	3989 (4)	617 (3)	2707 (5)	4.01
N4	4686 (4)	1191 (4)	4017 (6)	5.15
C19	4144 (5)	667 (5)	3850 (7)	4.66
C20	3783 (5)	201 (6)	4758 (7)	6.75
C21	4511 (5)	1100 (5)	1991 (7)	5.25
C22	4090 (7)	1439 (8)	1017 (9)	12.18
C23	5143 (7)	540 (7)	1541 (11)	11.68
C24	4875 (6)	1602 (5)	2928 (7)	6.28
C25	4338 (9)	2342 (6)	3011 (11)	12.40
C26	5660 (7)	1844 (9)	2873 (9)	13.30

[a] Standard deviations in the last significant digits are given in parentheses.

angles of 25 reflections and are reported in Table I with other experimental parameters. Intensities of three standard reflections were measured after every 100 data and showed no decrease during the course of data collection. The data were corrected for Lorentz and polarization effects.

The monoclinic symmetry for $Mn(hfac)_2(NITMe)_2$ and $Mn(hfac)_2(NITPh)_2$ were confirmed by Weissenberg photographs.

Structure Solution and Refinement. Both crystal structures were solved by conventional Patterson and Fourier methods using the SHELX-76 package.[12] The manganese positions were determined by means of sharpened Patterson functions, and the phases provided by these heavy atoms were used for successive difference syntheses that revealed the positions of the remaining non-hydrogen atoms. Structure refinements were carried out by full-matrix least-squares methods, with anisotropic thermal parameters for all non-hydrogen atoms.

Table III. Positional Parameters ($\times 10^4$) and Temperature Factors ($Å^2 \times 10^3$) for the NITPh Adduct[a]

	x	y	z	B_{eq}
Mn	2304 (1)	830 (1)	2360 (1)	4.37
F1	−789 (4)	−234 (4)	501 (3)	4.65
F2	−522 (4)	1108 (4)	533 (3)	8.13
F3	−1188 (4)	492 (5)	1231 (3)	9.55
F4	2555 (7)	−1825 (5)	932 (6)	18.51
F5	3504 (11)	−976 (6)	681 (6)	44.08
F6	3854 (10)	−1427 (8)	1478 (5)	20.95
F7	5717 (5)	1437 (6)	3471 (3)	10.51
F8	5303 (5)	2030 (4)	4215 (3)	5.27
F9	5188 (6)	695 (5)	4146 (4)	6.31
F10	1243 (10)	3492 (5)	3058 (3)	40.94
F11	1974 (7)	3415 (5)	3923 (4)	16.03
F12	596 (6)	2763 (5)	3669 (5)	26.74
O1	936 (4)	857 (3)	1645 (2)	5.12
O2	2985 (4)	−7 (3)	1760 (2)	5.58
O3	3622 (4)	842 (3)	3104 (2)	4.08
O4	1579 (4)	1718 (3)	2910 (2)	5.47
O5	1681 (4)	−351 (3)	2667 (2)	4.81
O6	3087 (4)	1969 (3)	2083 (2)	5.66
O7	964 (5)	−968 (4)	4578 (2)	8.72
O8	4065 (6)	2728 (5)	262 (3)	15.95
N1	1756 (4)	−664 (4)	3208 (3)	3.80
N2	1423 (5)	−943 (4)	4113 (3)	5.54
N3	3096 (5)	2322 (4)	1558 (3)	4.89
N4	3540 (6)	2665 (5)	694 (3)	9.48
C1	699 (7)	310 (5)	1234 (3)	5.07
C2	1345 (7)	−338 (6)	1066 (4)	5.84
C3	2442 (7)	−436 (5)	1351 (4)	7.57
C4	−459 (7)	409 (6)	878 (4)	5.65
C5	3048 (8)	−1158 (7)	1098 (6)	12.65
C6	3833 (7)	1436 (6)	3483 (3)	4.79
C7	3155 (8)	2106 (6)	316 (4)	4.67
C8	2082 (8)	2180 (5)	3316 (3)	7.42
C9	5019 (8)	1398 (7)	3830 (5)	4.21
C10	1429 (8)	2960 (7)	3459 (4)	8.70
C11	2481 (6)	−1426 (5)	3410 (4)	5.32
C12	2500 (6)	−1398 (5)	4103 (4)	6.06
C13	1097 (6)	−466 (5)	3610 (3)	3.43
C14	3598 (6)	−1312 (6)	3213 (4)	9.19
C15	1876 (7)	−2210 (5)	3085 (4)	5.34
C16	3389 (6)	−815 (6)	4443 (4)	5.66
C17	2504 (8)	−2274 (5)	4411 (4)	13.48
C18	182 (6)	130 (5)	3515 (3)	4.27
C19	−392 (6)	283 (5)	2925 (4)	5.97
C20	−1261 (6)	861 (6)	2845 (4)	7.32
C21	−1580 (7)	1280 (6)	3320 (5)	10.53
C22	−1027 (8)	1129 (6)	3905 (5)	9.35
C23	−133 (7)	549 (5)	4007 (4)	6.85
C24	2478 (7)	3149 (6)	695 (4)	7.68
C25	2412 (6)	3114 (5)	1375 (4)	6.60
C26	3788 (6)	2140 (5)	1183 (3)	5.84
C27	2561 (9)	4043 (6)	429 (5)	19.42
C28	1587 (7)	2619 (8)	308 (4)	9.91
C29	3016 (7)	3849 (5)	1754 (4)	7.40
C30	1267 (6)	3004 (5)	1520 (4)	9.78
C31	4664 (6)	1485 (5)	1279 (4)	7.57
C32	5138 (7)	1247 (6)	1866 (5)	8.85
C33	5947 (8)	633 (7)	1953 (6)	13.31
C34	6269 (9)	249 (8)	1468 (7)	15.02
C35	2826 (9)	483 (7)	871 (7)	15.96
C36	4995 (7)	1125 (6)	771 (5)	10.99

[a] Standard deviations in the last significant digits are given in parentheses.

Table IV. Selected Bond Distances (Å) for the NITMe Adduct[a]

Mn–O1	2.155 (4)	Mn–O7	2.127 (5)
Mn–O2	2.167 (5)	O5–N1	1.321 (8)
Mn–O3	2.176 (4)	O6–N2	1.282 (9)
Mn–O4	2.153 (5)	O7–N3	1.303 (7)
Mn–O5	2.122 (5)	O8–N4	1.276 (9)

[a] Standard deviations in the last significant digits are given in parentheses.

(9) Lamchen, M.; Wittag, T. W. *J. Chem. Soc. C* **1966**, 2300.
(10) Ullman, E. F.; Call, L.; Osiecki, J. H. *J. Org. Chem.* **1970**, *35*, 3623.
(11) Cotton, F. A.; Holm, R. H. *J. Am. Chem. Soc.* **1960**, *82*, 2979.
(12) (a) Sheldrick, G. "SHELX 76 System of Computing Programs"; University of Cambridge: Cambridge, England, 1976. (b) Busing, W. R.; Martin, K. O.; Levy, H. A. *Oak Ridge Natl. Lab. [Rep.], ORNL (U.S.)* **1971**, *ORNL*-594-32.

Table V. Selected Bond Distances (Å) for the NITPh Adduct[a]

Mn–O1	2.119 (4)	Mn–O6	2.154 (5)
Mn–O2	2.145 (5)	O5–N1	1.297 (8)
Mn–O3	2.120 (4)	O6–N3	1.302 (8)
Mn–O4	2.145 (5)	O7–N2	1.273 (8)
Mn–O5	2.144 (5)	O8–N4	1.261 (10)

[a] Standard deviations in the last significant digits are given in parentheses.

Table VI. Selected Bond Angles (deg) for the NITMe Adduct[a]

O1–Mn–O2	81.3 (2)	O2–Mn–O7	91.5 (2)
O1–Mn–O3	175.4 (2)	O3–Mn–O4	81.1 (2)
O1–Mn–O4	98.0 (2)	O3–Mn–O5	95.3 (1)
O1–Mn–O5	89.3 (1)	O3–Mn–O7	87.5 (1)
O1–Mn–O7	93.1 (1)	O4–Mn–O5	93.4 (2)
O2–Mn–O3	94.1 (2)	O4–Mn–O7	168.2 (2)
O2–Mn–O4	86.1 (2)	O5–Mn–O7	90.9 (2)
O2–Mn–O5	170.4 (2)		

[a] Standard deviations in the last significant digits are given in parentheses.

For both compounds the final refinement model included all hydrogen atoms in fixed and idealized positions.

Atomic positional parameters for $Mn(hfac)_2(NITMe)_2$ and $Mn(hfac)_2(NITPh)_2$ are listed in Tables II and III. Selected bond distances and angles are listed in Tables IV–VII.

Magnetic Susceptibility Measurements. Magnetic susceptibilities for the two title compounds were measured in the temperature range 300–6 K on an SHE superconducting SQUID susceptometer at a field strength of 0.5 T. Data were corrected for the magnetization of the sample holder and for diamagnetic contributions, which were estimated from the Pascal constants.

Electron Paramagnetic Resonance Measurements. EPR spectra of $Mn(hfac)_2(NITPh)_2$ and $Mn(hfac)_2(NITMe)_2$ were recorded with a Bruker ER200 spectrometer and a Varian E9 spectrometer operating at X- and Q-band, respectively. Liquid-nitrogen-temperature (77 K) spectra were obtained at X-band frequency by using a cold finger, while at 35 GHz the samples were cooled down only to 140 K.

Calculations. The molecular orbital analysis of the exchange pathways for the trans adducts of manganese follows the same scheme we used for the axial adducts of copper hexafluoroacetylacetonate:[8] a square-planar fragment containing the metal ion is allowed to interact with one radical in the axial position. The geometrical parameters that are relevant to this type of analysis are the metal–oxygen distance and the three Euler angles, ψ, θ, and ϕ, necessary to bring into coincidence a fixed reference frame on manganese and a mobile one on the nitroxide. When the direction of the bond between the manganese(II) ion and the oxygen atom of the nitroxide is orthogonal to the equatorial plane, ϕ is the angle of the projection of the O–N bond in the xy plane with the x axis, θ is the angle of the O–N bond with the perpendicular to the plane, and ψ is the dihedral angle between the Mn–O–N and the nitroxide planes. The most general case has been previously defined.[8] Besides the MnF_4^{2-} fragment used in a first approximation sample calculation the fragments A and B were used as models for the $Mn(hfac)_2$ unit in the cis and trans

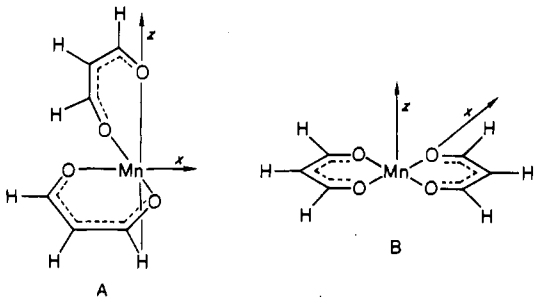

adducts, respectively, and the model molecules C and D were used for

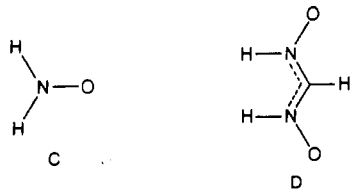

Table VII. Selected Bond Angles (deg) for the NITPh Adduct[a]

O1–Mn–O2	83.3 (1)	O2–Mn–O6	93.9 (2)
O1–Mn–O3	176.9 (2)	O3–Mn–O4	83.1 (1)
O1–Mn–O4	93.8 (1)	O3–Mn–O5	91.3 (1)
O1–Mn–O5	88.7 (1)	O3–Mn–O6	84.2 (1)
O1–Mn–O6	95.9 (1)	O4–Mn–O5	98.8 (2)
O2–Mn–O3	99.8 (1)	O4–Mn–O6	84.0 (1)
O2–Mn–O4	176.3 (1)	O5–Mn–O6	174.5 (1)
O2–Mn–O5	83.6 (1)		

[a] Standard deviation in the last significant digits are given in parentheses.

Table VIII. Geometrical, Magnetic, and Molecular Orbital Parameters for $Mn(hfac)_2(radical)_2$ Complexes

	r_a	ψ^b	θ^b	ϕ^b	J^c	S^d	ref
			Trans Adducts				
$M(hfac)_2$-(TEMPO)$_2$	2.127 (4)	38.6	12.8	25.5	158	4.8	6
$Mn(hfac)_2$-(PROXYL)$_2$	2.150 (4)	79.6	34.7	14.0	210	19.7	6
$Mn(hfac)_2$-(NITPh)$_2$	2.144 (5)	77.2	49.5	29.8	180	9.8	this work
	2.154 (5)	81.4	47.1	27.9			
			Cis Adduct				
$Mn(hfac)_2$-(NITMe)$_2$	2.122 (5)	86.6	52.0	80.7	187	13.2	this work
	2.127 (5)	83.0	48.9	7.2			

[a] In Å. [b] In deg. [c] In cm^{-1}. [d] The value is given multiplied by 10^4.

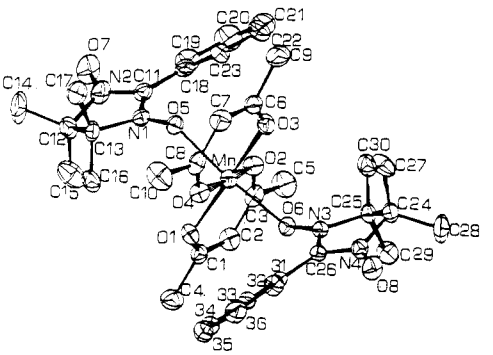

Figure 1. Molecular structure of $Mn(hfac)_2(NITPh)_2$.

the nitroxide and the nitronyl nitroxide ligands, respectively. The calculations were performed by using an idealized structure of the complexes, in which, however, the radical ligands are in the position determined by the actual experimental values of the Mn–O distances and of the angular parameters ψ, θ, and ϕ, with respect to the $Mn(hfac)_2$ moiety. In the case of the cis coordination geometry the angular parameters are defined analogously to the trans ones, the only difference being that the ψ and ϕ angles are indicative of a rotation around x instead of z.

The extended Hückel calculations were performed by using the fragment formalism,[13] on a IBM 4361/3 computer. For the manganese(II) ion double-ζ wave functions were used. The used Mn–O (nitronyl nitroxide) distances were those experimentally determined by X-ray diffraction (see Table VIII), while the other interatomic distances were as follows: in the radical unit, N–O = 1.29 Å, C–N = 1.32 Å, N–H = 1.00 Å, and C–H = 1.02 Å; in the $Mn(hfac)_2$ moiety (see models A and B), Mn–O = 2.15 Å, C–O = 1.24 Å, C–C = 1.50 Å, and C–H = 1.02 Å. The Mn–F distance in the MnF_4^{2-} unit was 2.0 Å.

Results

Description of the Structures. The crystal structures of both adducts comprise discrete octahedral $Mn(hfac)_2(NITR)_2$ molecules, but the NITPh is a trans and the NITMe is a cis derivative. The metal atoms are bound to two chelating hfac ligands and to two monodentate nitroxides in a distorted octahedral configuration. Views of the molecular structures of the two adducts are shown in Figures 1 and 2.

The distortions from regular octahedral geometry are rather small around manganese in $Mn(hfac)_2(NITPh)_2$. The Mn–O bond distances lie within the range 2.120 (4)–2.154 (5) Å, like

(13) Hoffmann, R. H.; Fujimoto, H.; Swanson, J. R.; Wan, C. C. *J. Am. Chem. Soc.* **1973**, *95*, 7644.

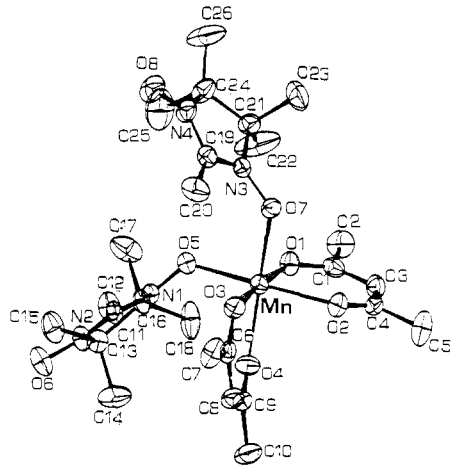

Figure 2. Molecular structure of $Mn(hfac)_2(NITMe)_2$.

in $Mn(hfac)_2(TEMPO)_2$ and $Mn(hfac)_2(PROXYL)_2$.[6] The hfac moieties are essentially planar, the largest deviation from the mean plane being 0.02 Å. The planes of the two hexafluoroacetylacetonates are almost parallel to each other, making an angle of about 20° with the equatorial plane. The two O–N bond distances in each nitroxide are asymmetric, the one corresponding to the oxygen atoms bound to the metal ion being longer than the other, as usual.[4,5] The two radicals show slightly different conformations. In one radical the C12 atom is 0.45 Å out of the plane of the O6–N1–C11–C13–N2–O7 atoms, while in the other nitronyl nitroxide unit only the O6–N3–C26–N4–O8 atoms lie on a plane, the C24 and C25 atoms being out of that plane by 0.46 and –0.13 Å, respectively. The phenyl rings are completely planar and make angles of about 22 and 21° with the mean plane of the corresponding NIT moieties.

The shortest N–O···N–O contacts, of 4.45 (5) Å, are found between the O7 oxygen atoms, which have relative positional parameters (x, y, z) and $(-x, -y, 1 - z)$.

The Mn–O bond distances in the coordination environment of $Mn(hfac)_2(NITMe)_2$ are on average 2.150 (5) Å, longer than in $Mn(hfac)_2(NITPh)_2$, 2.138 (5) Å. Also in this case the N–O bond distances of the groups not directly bound to manganese are shorter than the others. In the two radicals the O–N–C–N–O moieties are planar with the other two carbon atoms of the five-membered rings deviating from the plane by 0.13 and –0.14 Å in one nitronyl nitroxide and 0.08 and –0.14 Å in the other. The two hfac moieites are essentially planar, the largest deviation from the mean plane being 0.03 Å, and their mean planes make a dihedral angle of 75°.

The shortest N–O···N–O contacts of 4.80 (5) Å are found between the O8 oxygen atoms, which have relative positional parameters (x, y, z) and $(2 - x, 1 - y, -z)$.

Magnetic and EPR Results. The room temperature values of χT are 2.65 emu mol^{-1} K for $Mn(hfac)_2(NITMe)_2$ and 2.55 emu mol^{-1} K for $Mn(hfac)_2(NITPh)_2$, much lower than the 5.125 emu mol^{-1} K calculated for noncoupled systems, indicating strong antiferromagnetic interactions. Both complexes follow qualitatively the same behavior, χT decreasing with decreasing temperature as shown in Figures 3 and 4 and leveling off at about 1.9 emu mol^{-1} K for $Mn(hfac)_2(NITPh)_2$ and 2.0 emu mol^{-1} K for $Mn(hfac)_2(NITMe)_2$. At very low temperatures the χT curve for $Mn(hfac)_2(NITMe)_2$ shows a slight increase in χT, presumably due to weak intermolecular interactions. The corresponding curve for $Mn(hfac)_2(NITPh)_2$, on the other hand, keeps decreasing down to the lowest temperature we reached. The χ^{-1} vs T curves yield straight lines below 120 K, with C = 2.082 emu mol^{-1} K for $Mn(hfac)_2(NITPh)_2$ and C = 2.135 emu mol^{-1} K for $Mn(hfac)_2(NITMe)_2$ in agreement with a $S = {}^3/_2$ ground state.

The polycrystalline powder EPR spectra of $Mn(hfac)_2(NITPh)_2$ recorded at X-band frequency (room-temperature spectrum, Figure 5) are strongly temperature dependent: at high temperature many overlapping features are spread out in the field range 0–0.6 T, while at 77 K a very broad spectrum is observed with a clear

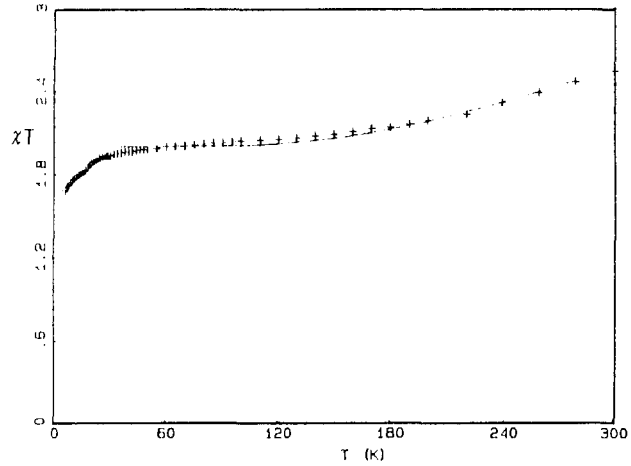

Figure 3. Temperature dependence of the magnetic susceptibility for $Mn(hfac)_2(NITPh)_2$ in the form χT (emu mol^{-1} K) vs T (K). The full line represents the best fit (see text).

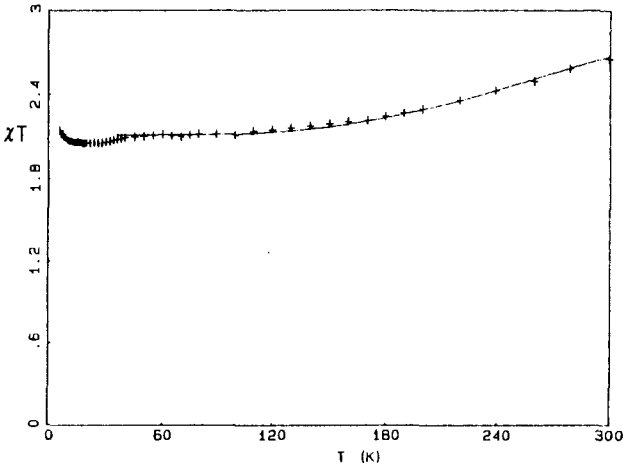

Figure 4. Temperature dependence of the magnetic susceptibility for $Mn(hfac)_2(NITMe)_2$ in the form χT (emu mol^{-1} K) vs T (K). The full line represents the best fit (see text).

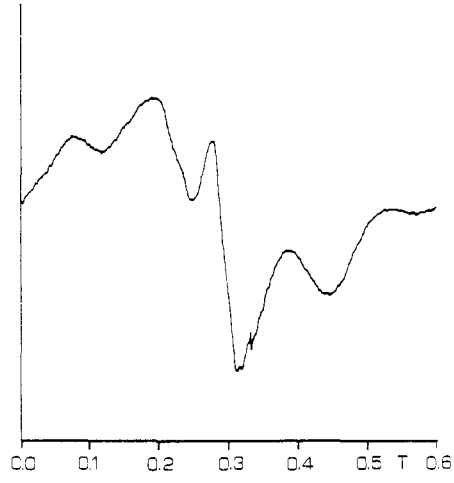

Figure 5. Polycrystalline powder EPR spectrum of $Mn(hfac)_2(NITPh)_2$ at X-band frequency at room temperature.

feature in the g = 4 region. The spectra look like those previously reported[7] for $Mn(hfac)_2(TEMPO)_2$ and $Mn(hfac)_2(PROXYL)_2$ as confirmed also by the similarity of the Q-band room-temperature data.

The polycrystalline powder EPR spectra of $Mn(hfac)_2(NITMe)_2$ show less dramatic variations with the temperature. Only one signal is observed at room temperature, at both X- (Figure 6) and Q-band frequencies, centered at g = 2.01. The line width is, within experimental error, equal at the two frequencies, with

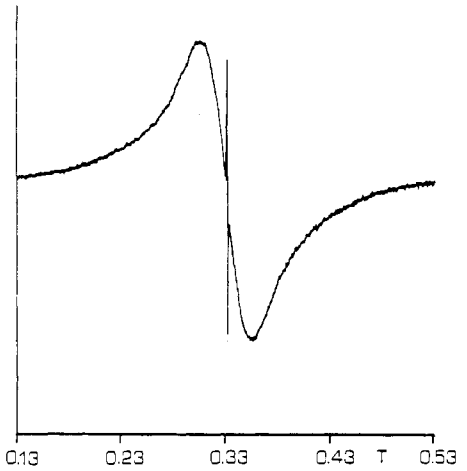

Figure 6. Polycrystalline powder EPR spectrum of $Mn(hfac)_2(NITMe)_2$ at X-band frequency at room temperature.

a peak-to peak width, ΔB_{pp}, of 480 G. When the sample is cooled down to liquid-nitrogen temperature (77 K), the spectra show two very weak additional features at low fields, but the main band remains substantially unchanged, with $g = 2.01$ and $\Delta B_{pp} = 480$ G.

Discussion

The discussion of the magnetic properties of $Mn(hfac)_2(NITPh)_2$ and $Mn(hfac)_2(NITMe)_2$ can proceed from the simple formula valid for symmetric three-spin clusters[14,15] with spins $^1/_2$–$^5/_2$–$^1/_2$ including only nearest-neighbor interactions. Attempts to fit the experimental χT curves for the two complexes yielded $J = 180$ cm^{-1}, $g = 2.06$, and $R = 1.45 \times 10^{-2}$ for $Mn(hfac)_2(NITPh)_2$ and $J = 187$ cm^{-1}, $g = 2.12$, and $R = 6.7 \times 10^{-3}$ for $Mn(hfac)_2(NITMe)_2$. R is defined as $\sum_i(\chi T_{oss} - \chi T_{calcd})^2/(\chi T_{oss})^2$. The calculated curves are shown in Figures 3 and 4. For both complexes we fitted the data in the range 30–300 K, avoiding the points at lower temperatures, where intermolecular couplings and/or impurities determine deviations from the behavior expected for the three spin cluster. The g values are slightly higher than the free-electron g value expected for manganese–radical species. This may be an artifact of the fitting procedure, which attributes to g the systematic errors that may be present in the experimental data.

Since in the two complexes the two radicals are not symmetrically bound to the manganese(II) ion, we considered how the calculated susceptibilities are affected by including two different coupling constants between the metal and the radicals, J' and J''. Sample calculations showed that small deviations from the average cause little effects; i.e., fitting with two constants or with their average is not much different. Therefore we felt it safer to avoid unnecessary complications and to stay at the fit with one J value because the experimental points above the low-temperature limit are relatively few and they do not allow the significant determination of two constants that are expected to be not too much different from each other.

The EPR spectra of $Mn(hfac)_2(NITPh)_2$ can be interpreted by using those previously reported[7] for $Mn(hfac)_2(TEMPO)_2$, which, as we noted above, are very similar. The low-temperature spectra correspond to the ground quartet state, which is split in zero-field by an amount larger than the X-band microwave quantum. The value of $D = 0.6$ cm^{-1} obtained from the single-crystal analysis of $Mn(hfac)_2(TEMPO)_2$ can also be used as a reasonable approximation to the zero-field splitting in the present compound. The spectra at high temperature, on the other hand, are those of the first excited sextet, and again the zero-field-splitting parameter reported for $Mn(hfac)_2(TEMPO)_2$, $D = 0.075$ cm^{-1}, can be used as a reasonable guess for the value of the corresponding parameter here.

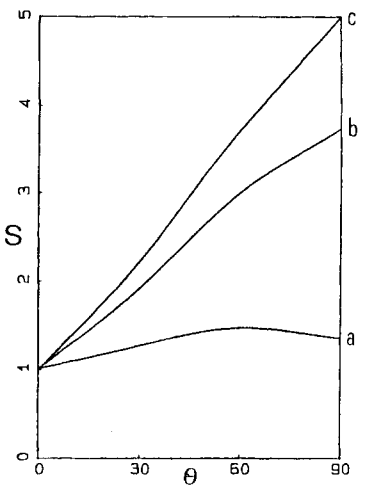

Figure 7. Variation of S vs θ (see text) with (a) $\psi = 30°$, (b) $\psi = 60°$, and (c) $\psi = 90°$.

The EPR spectra of $Mn(hfac)_2(NITMe)_2$ are less informative. No clear evidence of quartet and sextet states can be found because only one broad band is observed. If the spectra are those of isolated clusters, they tell us that the zero-field splitting is fairly small in both the ground and excited multiplets. This may be due to the fact that in the cis adduct the spin–spin contributions to D from the two radicals do not simply add to each other, because the principal axes of the respective **D** tensors are not identical.[16] An alternative explanation might rely on intermolecular exchange interactions, but it does not seem to be very probable, because magnetic data seem to indicate a stronger interaction for $Mn(hfac)_2(NITPh)_2$ than for $Mn(hfac)_2(NITMe)_2$.

In order to attempt to rationalize the nature of the exchange in manganese–nitroxide complexes, we used a simple extended Hückel approach. We assume that the observed coupling constant can be decomposed into a ferro- and an antiferromagnetic component[17,18] and that the overlap between the magnetic orbitals is indicative of the extent of the antiferromagnetic component of the coupling.[19] Following a procedure which is analogous to that previously suggested for copper dimers,[17,20] we assume that the variations of the coupling constants in a series of similar compounds can be reasonably accounted for by variations in the overlap between the magnetic orbitals. On the other hand, the ferromagnetic component cannot be easily introduced in this procedure; therefore, we will simply neglect it, on the assumption that it must be less rapidly varying with geometrical parameters, compared with the antiferromagnetic component. The assumption will have to be verified on the basis of the comparison with experimental data.

We performed preliminary sample calculations by using the fragment MnF_4^{2-} for the metal ion and H_2NO as a model ligand for an axial nitroxide in order to determine how the geometrical parameters affect the overlaps of the magnetic orbitals. For a given metal–oxygen distance the orbitals that can give sizable overlaps with the π^* orbital of the radical are z^2, xz, and yz, while the xy and $x^2 - y^2$ orbitals remain substantially orthogonal to it.

The exchange coupling constants for a manganese–radical species can be decomposed[21,22] according to

$$J = {}^1/_5 \sum_i J_{i,r}$$

(14) Gruber, S. J.; Harris, C. M.; Sinn, E. *J. Chem. Phys.* **1968**, *49*, 2183.
(15) Sinn, E. *Coord. Chem. Rev.* **1970**, *5*, 313.
(16) Gatteschi, D.; Bencini, A. In *Magneto-Structural Correlations in Exchange Coupled Systems*; Willet, R. D., Gatteschi, D., Kahn, O., Eds.; D. Reidel: Dordrecht, Holland, 1983; p 241.
(17) Hay, P. J.; Thibeault, J. C.; Hoffman, R. *J. Am. Chem. Soc.* **1975**, *97*, 4884.
(18) Kahn, O.; Briat, B. *J. Chem. Soc., Faraday Trans 1* **1976**, *72*, 268. Kahn, O.; Briat, B. *J. Chem. Soc., Faraday Trans 1* **1976**, *72*, 1441.
(19) Kahn, O. *Inorg. Chim. Acta* **1982**, *62*, 3.
(20) Bencini, A.; Gatteschi, D. *Inorg. Chim. Acta* **1978**, *31*, 11.
(21) Bominaar, E. L.; Block, R. *Phys. Rev. B: Condens. Matter* **1986**, *34*, 515.

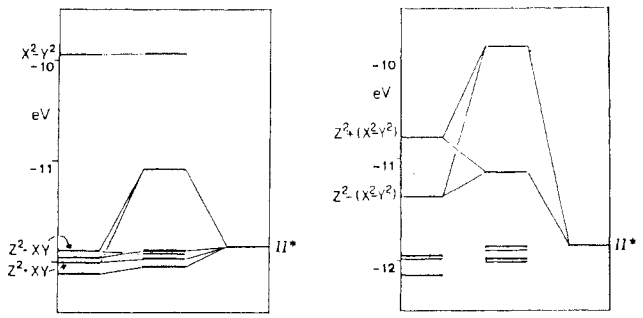

Figure 8. Extended Hückel molecular orbital diagrams: (a) Mn(hfac)$_2$(NITPh)$_2$; (b) Mn(hfac)$_2$(NITMe)$_2$.

where i represents magnetic orbitals that are essentially the d orbitals of the metal and r is the π^* magnetic orbital of the radical. Each individual $J_{i,r}$ constant has both a ferro- and an antiferromagnetic component. Since the energies of the z^2, xz, and yz orbitals of the square-planar fragment, which overlap significantly with the radical π^* orbital, are not too different from each other, we may use the sum of the squared overlap, $\sum S_{i,r}^2$, as a criterion for estimating the relative variation of J in the series.

In Figure 7 we plot $S = \sum S_{i,r}^2$ vs the angular parameters. When the Mn–O distance is shortened, the overlaps increase, making more intense both the ferro- and antiferromagnetic components. The parameter ϕ has substantially little effect on the sum of the squared overlaps. When θ is increased, the overlap increases, except for small values of ψ, whereas S actually decreases when θ is increased. Therefore, we may expect that the antiferromagnetic coupling increases when both θ and ψ are increased; indeed, if we compare the data reported in Table VIII for Mn(hfac)$_2$(TEMPO)$_2$ and Mn(hfac)$_2$(PROXYL)$_2$, we see that the latter has both θ and ψ larger than the former and a larger coupling constant. Therefore, these results seem to be encouraging us to continue in the analysis.

In order to have closer approximations to the true molecules and to attempt to rationalize the experimental results for all the Mn(hfac)$_2$(radical)$_2$ adducts thus far reported, we performed sample calculations by using fragments A–D shown in the Experimental Section. The values of the calculated S for the models of Mn(hfac)$_2$(TEMPO)$_2$ and Mn(hfac)$_2$(PROXYL)$_2$ are in the same order as the experimental J values, confirming the results suggested above, as shown in Table VIII.

If we compare Mn(hfac)$_2$(NITPh)$_2$ with Mn(hfac)$_2$(TEMPO)$_2$ and Mn(hfac)$_2$(PROXYL)$_2$, we see that the value of S for the first is intermediate between those of the other two and also that the exchange coupling constant is intermediate between the other two; therefore, it seems, notwithstanding the difference in the nature of the radicals, that S can be used as a good indicator of the extent of antiferromagnetic coupling. On the other hand since the geometrical parameters for Mn(hfac)$_2$(PROXYL)$_2$ and Mn(hfac)$_2$(NITPh)$_2$ are very similar, it must be concluded that the smaller overlap in the NITPh derivative is due to the delocalized structure of the ligand, suggesting that the coupling of nitronyl nitroxides may be weaker than that of nitroxides.

Comparing Mn(hfac)$_2$(NITPh)$_2$ with the cis adduct Mn(hfac)$_2$(NITMe)$_2$, we see that also in this case the order of S corresponds to the order of the coupling constants, although in this case the difference in the J values is rather small. In all the above discussion we have neglected the ferromagnetic component of J. It must not be identically zero, otherwise the spins would be coupled to give only a populated quartet ground state. However the satisfactory predictions reached by using only the antiferromagnetic component show that the role of the ferromagnetic component is still a minor one in the series of complexes we considered.

Acknowledgment. The financial support of the Italian Ministry of Public Education and the CNR is gratefully acknowledged.

Registry No. Mn(hfac)$_2$(NITPh)$_2$, 113533-12-3; Mn(hfac)$_2$(NITMe)$_2$, 113567-52-5; Mn(hfac)$_2$, 19648-86-3.

Supplementary Material Available: Anisotropic thermal parameters for the non-hydrogen atoms of Mn(hfac)$_2$(NITPh)$_2$ (Table SI), anisotropic thermal parameters for the non-hydrogen atoms of Mn(hfac)$_2$(NITMe)$_2$ (Table SII), complete listings of bond distances and angles for I (Tables SIV and SV) and II (Tables SVI and SVII), χT values for I and for II (Table SVIII), and parameters used in extended Hückel calculations (Table SIX) (20 pages); observed and calculated structure factors for I (Table SIII) and II (Table SX) (26 pages). Ordering information is given on any current masthead page.

(22) Eremin, M. V.; Rakitin, Yu. V. *Phys. Status Solidi B* **1977**, *80*, 579. Eremin, M. V.; Rakitin, Yu. V. *Phys. Status Solidi B* **1977**, *82*, 221.

Contribution from the Departments of Chemistry, University of Trondheim, Trondheim, Norway, The University of Reading, Whiteknights, Reading, Berkshire RG6 2AD, U.K., and Queen Mary College, The University of London, London, U.K.

Gas-Phase Electron Diffraction Study of Tetrakis(dimethylamido)zirconium(IV), Zr(NMe$_2$)$_4$

Kolbjørn Hagen,[1a] Catherine J. Holwill,[1b] David A. Rice,*[,1b] and Jonathan D. Runnacles[1c]

Received November 18, 1987

The molecular structure of Zr(NMe$_2$)$_4$ has been studied by gas-phase electron diffraction. The experimental data are fitted by a model that contains planar C$_2$N–Zr fragments bound to a ZrN$_4$ core that has a T_d symmetry. Small deviations from T_d symmetry cannot be excluded, but the deviation of the ∠N–Zr–N angle from the T_d value must be less than 5°. The lowest R factors were obtained with the ZrN$_4$ fragment having D_{2d} symmetry and with ∠N(1)–Zr–N(2) = 107.4 (48)°, but the difference from the tetrahedral model is not statistically significant. Two different values for the C(1)–N(1)–Zr–N(2) torsion angle (∠Φ_2) [109.7 (87)° and 127.7 (66)°] gave minima in the least-squares refinements with ∠Φ_2 = 109.7 (87)°, giving a slightly lower R factor, but the difference from that obtained with ∠Φ_2 = 127.7 (66)° was not statistically significant. The values, with estimates of uncertainties (2σ) for the principal distances (r_g) and angles ($\angle_\alpha$), are r(Zr–N(1)) = 2.071 (11) Å, r(C(1)–N(1)) = 1.461 (4) Å, r(C(1)–H(1)) = 1.118 (12) Å, ∠C(1)–N(1)–C(1^1) = 111.2 (11)°, and ∠N(1)–C(1)–H(1) = 108.7 (30)°, with ∠N(1)–Zr–N(2) being assumed as 109.47°.

Introduction

Tetrakis(dimethylamido) complexes, M(NMe$_2$)$_4$, have been isolated for a number of transition elements,[2] and thus they provide one of the few classes of compounds where it could be possible to determine the effect of d^n configuration upon structure. Examination of the metal–nitrogen stretching modes has led to the suggestion that the MN$_4$ fragment in a number of these M-

(1) (a) The University of Trondheim. (b) The University of Reading. (c) The University of London.

(2) Bradley, D. C. *Adv. Inorg. Chem. Radiochem.* **1972**, *15*, 259.

0020-1669/88/1327-2032$01.50/0